Influence of Structure on Electron Correlation Effects and Electron−Water Dispersion Interactions in Anionic Water Clusters

Christopher F. Williams and John M. Herbert*

Department of Chemistry, The Ohio State University, Columbus, Ohio 43210

Received: March 15, 2008; Revised Manuscript Received: April 17, 2008

Electronic structure calculations at the level of second-order Møller−Plesset perturbation theory have been performed on anionic water clusters, $(H_2O)_n^-$, in the $n = 14-33$ size regime. The contribution to the electron binding energy that arises from electron correlation is found to be significantly larger for cavity-bound electrons than it is for surface-bound electrons, even for surface states with electron binding energies well above 1 eV. A decomposition of the correlation energy into interactions between pairs of Boys-localized molecular orbitals is used to demonstrate that the larger correlation energy found in the cavity isomers arises from electron−water dispersion interactions, and that the dispersion interaction is larger in cavity-bound isomers because the unpaired electron penetrates well beyond the first solvation shell. In contrast, a surface-bound electron exhibits virtually no penetration into the interior of the cavity. To obtain a qualitatively accurate picture of this phenomenon, one must plot molecular orbitals using isoprobability surfaces rather than arbitrarily-selected isocontours.

I. Introduction

Water cluster anions, $(H_2O)_n^-$, have been the target of intense study, both as interesting species in their own right and to gain insight as to how the solvation shell surrounding an aqueous electron might be formed. Early measurements[1] of the vertical electron binding energies (VEBEs) of size-selected $(H_2O)_n^-$ clusters showed that VEBE $\propto n^{-1/3}$ for $n > 11$. Interpreted in terms of a simple continuum dielectric model,[2] the data for $n > 11$ suggest that the excess electron is surrounded by water molecules, forming a "cavity state" analogous to the bulk aqueous electron. More recent photoelectron spectra have revealed at least three different types of cluster isomers that have very different VEBEs.[3] In addition to the strongly-bound class of isomers observed originally, two weakly-bound classes were also detected. Presumably, these three classes of isomers represent different electron binding motifs; however, owing to the diverse morphology exhibited even by small water cluster anions,[4–11] a definitive assignment is a very challenging problem.

Despite this difficulty, the infrared (IR) spectra of the trimer,[12] tetramer,[13] and hexamer[14] cluster anions have been definitively assigned. In each case, the dominant isomer exhibits the so-called double acceptor ("AA") electron binding motif, in which two hydrogen atoms on the same water molecule—which do not participate in the intermolecular hydrogen-bonding network—solvate the extra electron. IR spectra suggest that the AA binding motif persists at least up to $n = 24$ and possibly beyond.[15–17] Interestingly, AA isomers dominate the IR spectra despite the fact that these isomers are often not the lowest energy geometries on the anion potential energy surface.[10,11,18] Clearly there are multiple factors that contribute to whether a particular isomer is observed in a molecular beam experiment, including the stability of a particular anionic cluster geometry, the electron affinity of the underlying neutral cluster, and the dynamical rearrangements that accompany electron attachment to a neutral cluster.

Theory stands to play a major role in elucidating the relationship between these factors. However, no fully-encapsulated cavity isomer of $(H_2O)_n^-$ has yet been reported for $n < 24$ [19–21] (although cavity-like "embryonts",[22] in which a partial solvation shell has formed, can be found in smaller clusters[23]); hence a comprehensive comparison of surface and cavity states of $(H_2O)_n^-$ is a challenging problem for ab initio calculations. Consequently, most of the insight into large water cluster anions has come from mixed quantum mechanics/molecular mechanics (QM/MM) simulations,[24–28] in which only the unpaired electron is treated quantum-mechanically. The electron−water pseudopotential is thus crucially important. In early studies, such potentials were developed in an ad hoc way,[29,30] though many of the assumptions that underlie them were later validated.[31,32] The surprising outcome of these simulations has been that the electron preferentially forms a surface state, and that there are no dynamically stable cavity states at all for $n < 200$, except at very low temperatures ($T \lesssim 50$ K).[24,33]

The electron−water pseudopotential employed in the aforementioned simulations accounts for electron−water polarization only in an averaged way, and neglects many-body dispersion interactions. For small dipole-bound anions, electron correlation effects are known to be responsible for a significant fraction of the VEBE,[34–37] and the Møller−Plesset perturbation series converges very slowly,[37] indicative of important high-order correlation effects. Gutowski and co-workers[36,37] have analyzed electron correlation in dipole-bound anions using a double perturbation expansion (and subsequent approximations) to isolate electron−molecule dispersion from the rest of the interaction energy. Dispersion is found to contribute significantly to the VEBE in weakly-bound anions, sometimes exceeding the contribution from electrostatic (charge-dipole) interactions. On the other hand, these studies focused on very small and *extremely* weakly-bound anions, such as $(HF)_2^-$, HCN^-, CH_3CN^-, $C_3H_2^-$, and $C_5H_2^-$, none of which has a VEBE greater than 0.1 eV.[34–37] Sommerfeld and Jordan,[38] however, have analyzed correlation effects in systems as large as $(H_2O)_{24}^-$ using a model Hamiltonian that includes electron−water dispersion interactions.[39] These authors report weak electron binding ($\lesssim$0.2 eV) in certain cluster isomers even when electrostatic interactions are completely removed from the model, i.e., using

* Corresponding author. E-mail: herbert@chemistry.ohio-state.edu.

10.1021/jp802272r CCC: $40.75
Published on Web 06/18/2008

only electron correlation to bind the electron.[38] Correlation effects thus seem to be important in large $(H_2O)_n^-$ clusters, but these effects have not yet been extensively quantified.

In this study, we examine electron correlation and many-body dispersion effects using ab initio calculations, in clusters as large as $(H_2O)_{33}^-$ that exhibit both surface states and cavity states, and where VEBEs exceed 2.0 eV for some isomers. Because density functional theory consistently overestimates VEBEs (by $\sim$ 0.5 eV in some cases),[20] the only tractable ab initio methodology amenable to clusters of this size is second-order Møller−Plesset perturbation theory (MP2). This method does not incorporate the high-order correlation effects that are qualitatively important in small, weakly-bound anions.[36,37] However, it has previously been shown that the MP2 method, combined with a highly diffuse (but otherwise modest) double-ζ basis set, recovers an essentially constant fraction of the correlation energy associated with the unpaired electron,[21] and thus affords semiquantitative predictions for VEBEs. This is especially true for cluster isomers with VEBEs larger than about 0.2 eV, where small-cluster benchmarks suggest an accuracy of $\sim$0.02−0.03 eV in the predicted VEBEs.[20,21] We will thus utilize MP2 calculations to analyze electron correlation effects (specifically, the electron−water dispersion interaction) in detail, focusing specifically on differences between surface states and cavity states.

II. Technical Details

An expanded database of small water cluster anions has been drawn up starting from that given in ref 21 and is included in the Supporting Information. Geometries were optimized at the B3LYP/6-31(+,3+)G* level (using the SG-1 quadrature grid[40]), with no constraints on point group symmetry. The 6-31(+,3+)G* basis[21] augments the standard 6-31++G* basis with two additional diffuse *s* functions on each hydrogen atom, whose exponents are decremented by successive factors of 3.32. (Additional diffuse functions on the oxygen atoms have only a very small effect on VEBEs.[20]) All calculations discussed use a drop tolerance of 10^{-14} au. Eigenvectors of the overlap matrix that correspond to eigenvalues smaller than 10^{-7} are projected out of the atomic orbital basis. Electronic structure calculations were performed using Q-Chem;[41] Molden[42] and Visual Molecular Dynamics[43] were used for the visualization of molecular structures and molecular orbitals (MOs).

For calculation of the VEBE,

$$\mathrm{VEBE} = E_{\mathrm{neutral}} - E_{\mathrm{anion}} \tag{1}$$

the MP2/6-31(+,3+)G* level of theory was used. Although double-ζ basis sets are generally unsuitable for correlated wavefunction calculations, in the case of $(H_2O)_n^-$ the valence orbitals of the water molecules undergo little relaxation following electron detachment,[20] therefore calculation of the VEBE using this basis set benefits from cancellation of errors. Calculations using this basis set have been benchmarked against the those using larger and more diffuse basis sets, at both the MP2 and CCSD(T) levels,[21] and it was concluded that the MP2/6-31(+,3+)G* method affords VEBEs that lie $\sim$ 0.01−0.02 eV below those obtained either at the CCSD(T)/6-31(+,3+)G* level or the complete-basis MP2 limit.

III. Results and Discussion

A. Benchmarking. Larger water cluster anions ($n > 24$) are of particular interest in this study as they are able to form both surface and cavity states. MP2 calculations for clusters of this size are very expensive, and it would be advantageous to perform these calculations with the modest 6-31(+,3+)G* basis set. Although double-ζ basis sets are not generally considered to be flexible enough for correlated wavefunction calculations, previous studies have found that this basis affords surprisingly good results for $(H_2O)_n^-$ VEBEs,[21] because there is little relaxation of the water valence orbitals upon electron detachment. To verify this, VEBEs are calculated for both the 6-311(+,3+)G** basis set and the 6-31(+,3+)G* basis set for a collection of small ($n \leq 7$) cluster isomers. It is found that the average difference between the two is only 0.030 eV (see Supporting Information).

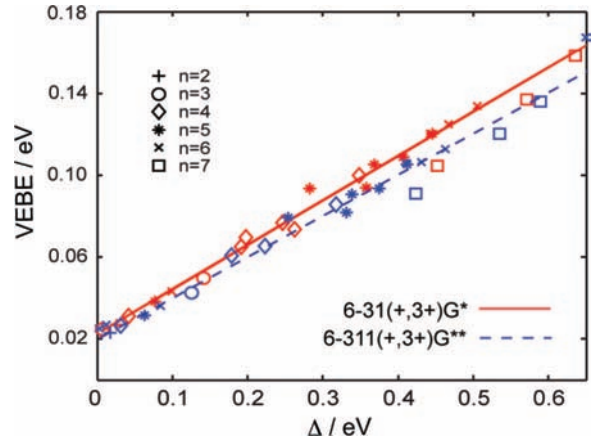

Figure 1. Plot of excess-electron correlation, energy Δ [as defined in (2)] against vertical electron binding energy (VEBE), for a database of water cluster anions calculated at both the MP2/6-31(+,3+)G** level and the MP2/6-311(+,3+)G** level. Both data sets show the same linear trend.

Electron correlation energy E_{corr} is an extensive property that increases with the number of electrons (and hence the number of water molecules). It is the correlation due to the unpaired "excess" electron that is of primary concern here. This is given by the intensive quantity

$$\Delta = E_{\mathrm{corr}}(\mathrm{neutral}) - E_{\mathrm{corr}}(\mathrm{anion}) \tag{2}$$

Note that $\Delta > 0$.[44] It has previously been observed that there is a linear relationship between Δ and the VEBE.[21] As this relationship will be of particular interest in this study, we would therefore like to verify that it is independent of basis set. Δ is plotted against VEBE in Figure 1 for both double- and triple-ζ basis sets and it is found that they both show a similar linear trend. This affirms previous results[18,20,21] that MP2/6−31(+,3+)G* calculations are sufficient for qualitative and semi-quantitative studies of electron correlation in water cluster anions.

B. Water Cluster Morphology. The morphology of water clusters has been the focus of intense study, and they have been classified into two broad types: cavity states, where the unpaired electron is surrounded and solvated by water molecules in a manner similar to the bulk aqueous electron, and surface states, wherein the electron is located on the surface of the water cluster. In ab initio calculations, the location of the unpaired electron can be seen by looking at the singly-occupied MO (SOMO), and Figure 2 shows a series of isoprobability surfaces that encompass ever greater fractions of the SOMO density, $|\phi_{\mathrm{SOMO}}(r)|^2$, for both a surface state and a cavity state. In both cases, the water molecules are arranged in a clathrate-like network,[45] and the two clusters are labeled (see Figure 2) according to the ring structure of the hydrogen-bonding network.[20,45] The blue and gray isosurfaces indicate positive and

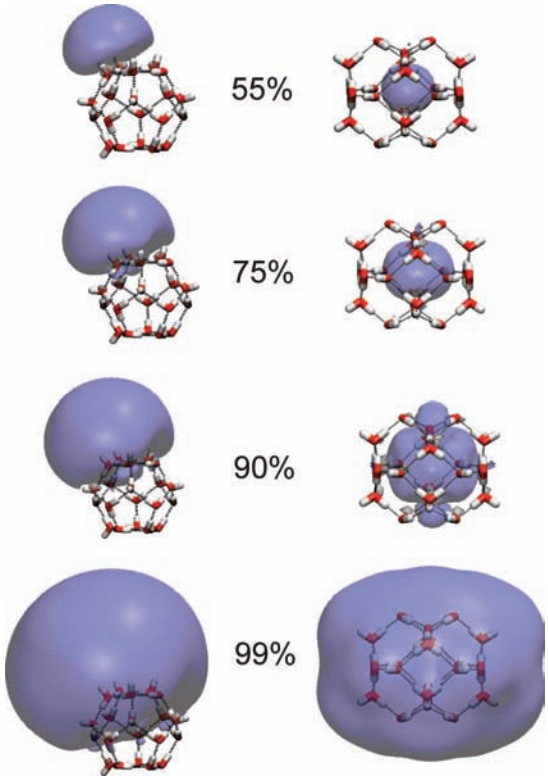

Figure 2. Series of isoprobability surfaces encompassing ever greater fractions of the SOMO, for a surface state and cavity state. The cavity state is $(H_2O)_{24}^-$ isomer 4^66^8B and the surface state is $(H_2O)_{20}^-$ isomer 5^{14}, both taken from ref 20. The blue isosurface shows the positive part of the wavefunction and the gray isosurface (barely visible) shows the negative part of the wavefunction.

negative parts of the orbital. (The latter are scarcely visible, as the SOMO has very little *p* character).

Deductions based on the Hartree−Fock orbitals make the assumption that that they are not qualitatively altered by electron correlations and also that the Hartree−Fock determinant is a good approximation to the true wavefunction. The first of these assumptions is true for most water cluster anions because Δ is numerically small, less than 0.2 eV for $n \leq 7$, and not greater than 0.6 eV even for the clusters up to $n = 33$ examined in this study. The second is true for electron-binding clusters where the SOMO has a negative eigenvalue, resulting in bound anion at the level of the Koopmans' Theorem approximation. As the number of valence electrons (i.e., the size of the water cluster) grows, so too does the polarization of the water cluster by the unpaired electron, and as a result the VEBE obtained using Koopmans' Theorem tends to increase with cluster size. (In fact, the Koopmans' Theorem estimate of the VEBE is a reasonable approximation to the MP2 result for larger clusters, e.g., $n \gtrsim 20$.) Because these larger clusters can form both surface and cavity states our investigation will focus on these.

For cavity states of $(H_2O)_n^-$, it is tempting to conceptualize the electron as being completely confined within the cavity, as for example in Figure 13b of ref 20. If we plot the SOMO using the same isocontour as used in that reference, we find that it encapsulates only 55% of the SOMO density (see Figure 2). If the isosurface is drawn so that it contains 90% of the integral of $|\phi_{SOMO}(r)|^2$, it is found that there is a substantial fraction of the SOMO has penetrated beyond the cavity. We note also that the SOMO for the cavity state has more *p* character than that of the surface state, and that the small gray (negative) parts of the SOMO are oriented along the O−H bonds of the four water

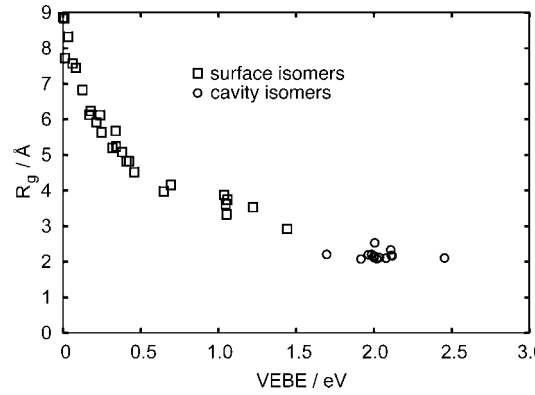

Figure 3. Plot of the radius of gyration of the SOMO [as defined in (3)] against VEBE, for a database of water cluster anions. Both are calculated at the Hartree−Fock/6-31(+,3+)G* level. The surface isomers show a decrease in the radius of gyration with an increase in the VEBE, in contrast to the cavity isomers.

molecules that interact directly with the unpaired electron. These can be attributed to the sp_3 orbitals containing the non-hydrogen-bonded lone pairs of the solvating water contributing to the SOMO. If the isosurface is drawn so that it contains 99% of the SOMO density, it is found that the SOMO completely encompasses the water cluster. This is in contrast to the SOMO of the surface isomer, which does not completely encompass the water cluster, even when the isosurface contains 99% of the SOMO density.

For surface isomers, the radius of gyration of the SOMO,

$$R_g = [\langle \varphi_{SOMO}|r^2|\varphi_{SOMO}\rangle - \langle \varphi_{SOMO}|r|\varphi_{SOMO}\rangle^2]^{1/2} \quad (3)$$

is closely correlated with the VEBE, as pointed out by Bartels[46] based a moment analysis of $(H_2O)_n^-$ absorption spectra.[47] Surface isomers with large VEBEs tend to exhibit small values of R_g, while those with small VEBEs have much larger SOMOs. This relationship is readily apparent in our calculations, and Figure 3 presents a plot of R_g versus VEBE for both surface and cavity isomers. For the surface isomers the radius of gyration decreases with increasing VEBE. This is not the case for cavity isomers, because the electron is mostly, although not completely, confined by the water molecules that form the cavity. The approximate radius of the cavity is 2 Å, consistent with the calculations of the cavity size in the bulk calculated by Turi et al.[28] The contraction of the SOMO with increasing VEBE for surface states results from the balance between kinetic and potential energy. A compact SOMO with small R_g has a large kinetic energy as a result of the curvature of the wavefunction, and this is only favorable if it is offset by the wavefunction's ability to sample deeper regions of the potential well, which are found nearby the water molecules.

C. Effect of Morphology on Electron Correlation. The correlation energy due to the unpaired electron has been calculated at the MP2/6−31(+,3+)G* level for a database of cluster isomers ranging from $n = 14$ to $n = 33$. (The full database of energies and geometries can be found in the Supporting Information.) Prior to this work, the largest $(H_2O)_n^-$ clusters examined with ab initio calculations were a few $n = 20$ and $n = 24$ isomers[19–21] obtained from clathrate-like[45] neutral clusters, followed by geometry optimization on the anionic potential surface. Several such isomers (taken from the database ref 21) are examined here as well, but to obtain a more diverse data set, we also examine clusters extracted from a QM/MM simulation of the sort mentioned in the Introduction.

The QM/MM simulation was performed on a stable cavity state of $(H_2O)_{216}^-$, using the Fourier gid method[48] to represent

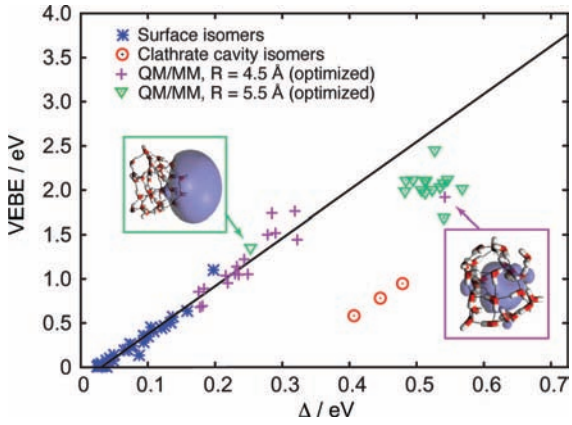

Figure 4. Plot of excess-electron correlation energy, Δ [as defined in (2)], against VEBE, for a database of water cluster anions. Both are calculated at the MP2/6-31(+,3+)G* level. The cavity isomers show a larger contribution to the VEBE arising from electron correlation.

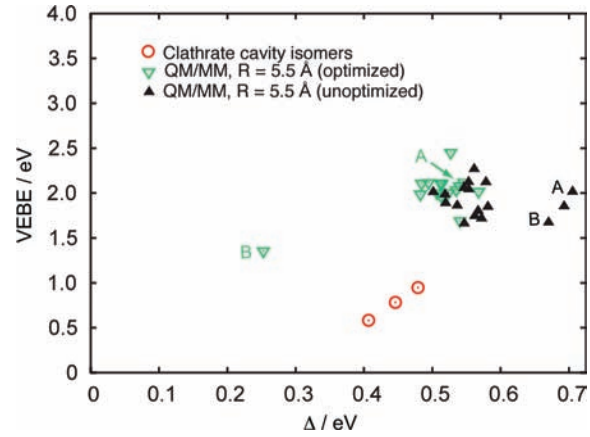

Figure 5. Plot of excess-electron correlation energy, Δ, against VEBE, for the cavity state anions only. Both quantities are calculated at the MP2/6-31(+,3+)G* level. Both the unoptimized clusters carved out of the QM/MM simulation with $R = 5.5$ Å and their optimized forms are shown. In general the optimization process decreases the electron correlation contribution to the VEBE, because the optimized structures reduce the radius of gyration of the SOMO, thus reducing the number of water molecules with which it interacts strongly. This effect is particularly pronounced in the state labeled B, which optimizes to a surface state (see Figure 6).

the wavefunction of the unpaired electron and the pseudopotential of Turi and Borgis[32] to model the electron−water interaction. (This pseudopotential has been used in many recent simulations of large, anionic water clusters.[24,27,28]) Classical equations of motion for the flexible water molecules were propagated using Hellmann-Feynman forces on the ground-state adiabatic potential obtained from the one-electron Hamiltonian. The simulation was equilibrated for 30 ps at $T = 300$ K, followed by a production run of an additional 20 ps. Smaller clusters for the database were extracted from this production run, at intervals of 1 ps, by selecting all water molecules within a specified radius of the centroid of the one-electron wavefunction. Two such radii were used: $R = 4.5$ Å, which yielded clusters ranging from $n = 18$ to 24; and $R = 5.5$ Å, which afforded clusters in the range $n = 29$ to 33. The geometries of these clusters were then optimized, again using the Fourier Grid/pseudopotential method. The values $R = 4.5$ Å and $R = 5.5$ Å were selected because the optimized geometries in the latter case are mostly cavity states and the optimized geometries in the former case are primarily surface states, with one exception in either case, as discussed below.

Figure 4 shows the excess-electron correlation energy Δ as a function of VEBE, for all of the clusters in the aforementioned database. The quantity Δ turns out to be a very good indicator of whether a particular isomer has a surface- or a cavity-type morphology, as the latter are associated with a much larger ratio of Δ to VEBE. This indicates that, for cavity states, a much greater portion of the VEBE arises from electron correlation than it does in the case of surface states, because

$$\mathrm{VEBE} = E^{\mathrm{HF}}_{\mathrm{neutral}} - E^{\mathrm{HF}}_{\mathrm{anion}} + \Delta \qquad (4)$$

where $E^{\mathrm{HF}}_{\mathrm{neutral}}$ and $E^{\mathrm{HF}}_{\mathrm{anion}}$ are the Hartree−Fock energies of the neutral and anionic clusters. With regard to the pseudopotential-optimized geometries, the two exceptional cases noted above (the $R = 4.5$ Å cavity state and the $R = 5.5$ Å surface state) conform perfectly to this trend.

The surface isomers show a continuation of the linear relationship between the VEBE and the correlation energy for the unpaired electron, as was first seen in Figure 1 for the smaller surface isomers, whereas the cavity isomers do not show this trend. This means that for surface isomers an approximately constant portion of the VEBE is due to the correlation of the excess electron with the valence electrons of the water cluster. This is not surprising, because an increase in VEBE correlates with an excess-electron wavefunction that is bound closer and more tightly to the water cluster (cf. Figure 3), in which case one would expect an increase in Δ. Why it should be so close to linear, however, is not obvious to us.

The cavity isomers from the QM/MM simulations tend to show a higher VEBE compared to the clathrate isomers. This is probably because the asymmetry of the QM/MM isomers tended to produce clusters with a moderate dipole moment, ranging from 4−18 D in the neutral form, so in addition to dispersion-like electron correlation effects there is also strong electrostatic binding of the electron. This is in contrast to the clathrate isomers of similar size, which have dipole moments close to zero because of their high symmetry. The clathrate isomer group also includes one $n = 14$ isomer that was taken from the literature,[23] and having a dipole moment of 9 D, but also a low VEBE compared with the QM/MM cavity isomers. This apparently anomalously low binding energy could be due to the fact that this is a very high energy isomer on the anion potential surface.

The $R = 4.5$ Å clusters extracted from $(H_2O)_{216}^-$ show significant gaps in their hydrogen-bonding networks and thus tend to undergo significant relaxation upon geometry optimization, unlike the $R = 5.5$ Å clusters that consist of nearly a complete solvation shell and are much closer to being stable structures when extracted from the simulation. A plot of excess-electron correlation energy, Δ, against VEBE is shown in Figure 5 for the cavity states only. For the $R = 5.5$ Å clusters carved from the QM/MM simulation, both optimized and unoptimized geometries are shown. For three of these geometries, Δ make an especially large contribution to the VEBE. These three clusters possess SOMOs that encompass unusually large numbers of water molecules. In all cases the number of waters encompassed by the SOMO is reduced upon geometry optimization; however, the isomer labeled B shows a dramatic decrease in the portion of its VEBE due to electron correlation. Examination of the structures as shown in Figure 6 leads to a conclusion that might have been anticipated from the results in Figure 4. In the case of Figure 6b, the radius of gyration of the SOMO is so large that upon optimization, the electron "escapes" to form a surface-type isomer. The number of water molecules

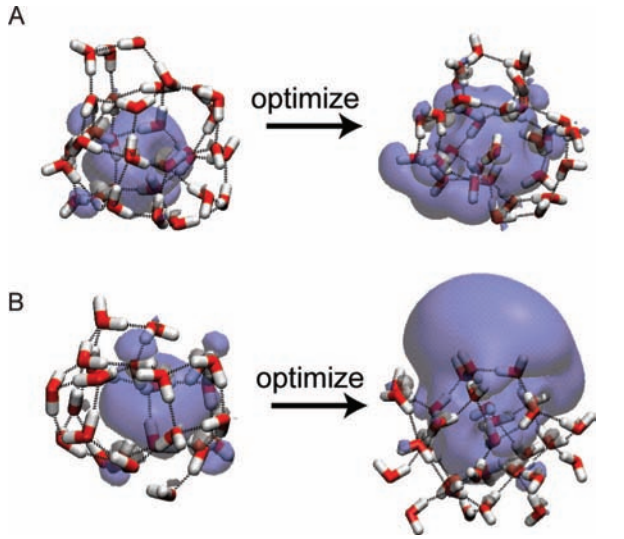

Figure 6. Outliers in which the correlation energy for the unpaired electron, Δ, makes an unusually large contribution to the VEBE. The unoptimized forms have a SOMO that encompasses an unusually large number of water molecules. This is reduced in both cases by optimization, but considerably more for B than A. Hence the dramatic change in the portion of VEBE due to electron correlation that is evident in Figure 5.

encompassed by the SOMO is reduced by optimization in both A and B, but considerably more for the latter, which optimizes to a surface state, than for the former, which optimizes to a cavity state. The outlier B, then, further reinforces the notion that the magnitude of Δ is an indicator of binding motif.

D. Dispersion Energy. Within the context of MP2 theory, the total electron correlation energy $E_{\text{corr}}^{\text{MP2}}$ can be expressed as a sum of pair correlation energies (PCEs),

$$E_{\text{corr}}^{\text{MP2}} = \sum_{i<j} E_{ij}^{\text{PCE}} \tag{5}$$

each of which is given by

$$E_{ij}^{\text{PCE}} = \sum_{a<b} \frac{|\langle \varphi_i \varphi_j || \varphi_a \varphi_b \rangle|^2}{\varepsilon_i + \varepsilon_j - \varepsilon_a - \varepsilon_b} \tag{6}$$

The notation here is standard: ϕ_i and ϕ_j denote occupied Hartree−Fock orbitals (with corresponding eigenvalues ε_i and ε_j) and ϕ_a and ϕ_b are virtual Hartree−Fock orbitals (with eigenvalues ε_a and ε_b). Because dispersion is due to mutual correlation of charge clouds, the dispersion energy between the water cluster and the unpaired electron can be defined as the sum of all double excitation energies involving the SOMO and one other occupied orbital. We refer to these particular PCEs $E_{i,\text{SOMO}}^{\text{PCE}}$ as SOMO pair correlation energies (SPCEs), and the sum of all SPCEs [i.e., all terms in (6) for which j = SOMO] defines the electron−water dispersion energy at the MP2 level,

$$E_{\text{e-disp}}^{\text{MP2}} = \sum_{i \neq \text{SOMO}} E_{i,\text{SOMO}}^{\text{PCE}} \tag{7}$$

This definition of electron−water dispersion is equivalent to that proposed for dipole-bound anions in general by Gutowski et al.,[36] where it was motivated using a double perturbation expansion.

Decompositions of the MP2 correlation energy were examined in detail for a clathrate-like isomer of $(H_2O)_{24}^-$, in which the electron is bound in a cavity with a VEBE of 1.1 eV, and also a clathrate-like isomer of $(H_2O)_{20}^-$ in which the electron is

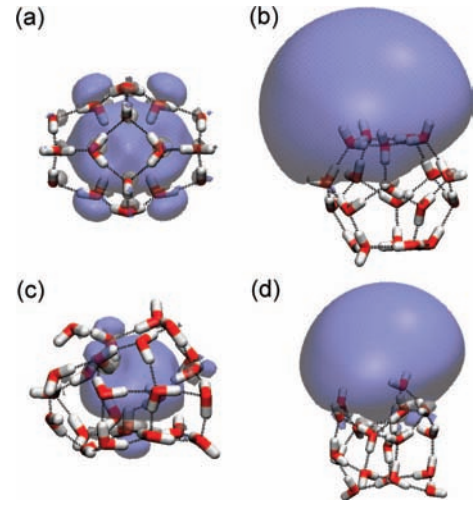

Figure 7. Isoprobability surfaces encompassing 90% of $|\phi_{\text{SOMO}}|^2$ for (a) $(H_2O)_{24}^-$ isomer $4^6 6^8$B, (b) $(H_2O)_{20}^-$ isomer 5^{14}, (c) a cavity state extracted from a QM/MM simulation, and (d) a surface state extracted from a QM/MM simulation. The blue and gray isosurfaces represent the positive and negative lobes of ϕ_{SOMO}.

bound at the surface, with a VEBE of 0.9 eV. The geometries and canonical SOMOs of these are shown in Figure 7a,b, respectively. The total electron−water dispersion energy, as defined in eq 7, is 0.67 eV for the cavity state and 0.27 eV for the surface state. The numerator in eq 6 suggests that an explanation for this could be sought by looking at the distance between the different valence orbitals of the cluster and the SOMO (because this should correlate with their Coulomb interaction), but it is difficult to derive any intuitive chemical picture from the canonical Hartree−Fock MOs, and thus a representation wherein the MO are more localized on the water molecules would be helpful. The Boys localization procedure[49] is one way of finding such a representation, by minimizing the sum of the variances of the MOs.

Histograms of the SPCEs, obtained in the basis of Boys-localized MOs, are shown in Figure 8 for each of the two isomers mentioned above. It is found not only that the cavity state has a wider range of SPCEs than the surface isomer, but also that the SPCEs have a markedly different distribution. The surface isomer shows a large number of orbitals in the lowest range of SPCE, in fact the majority of orbitals fall into this category. In contrast, the cavity state has far more orbitals that have a medium amount of SPCE. A explanation is suggested by examination of the Boys orbitals of the two isomers, a few of which are shown in Figure 9. The SOMOs (depicted in yellow and green in Figure 9) are not greatly affected by the localization procedure, in contrast to the orbitals of the water molecules. In the Boys-localized basis, the MOs associated with the largest SPCEs are those located in close proximity to the SOMO (for both surface and cavity states), and the Boys MOs with the lowest SPCEs are localized a much greater distance away from the SOMO. As was demonstrated by Figure 2, the spacial overlap between the water cluster itself and the SOMO is much smaller in the surface states, therefore there are a large number of orbitals that are a long distance away from the SOMO. In contrast, because the cavity isomer confines the SOMO within the water cluster the majority of the orbitals on the water cluster are close to the SOMO. This explains the large number of orbitals with relatively large SPCEs in the case of the cavity state, for in this case the SOMO simply overlaps more water molecules than in the case of the surface state. In the case of the cavity isomer there seems to be a particular correlation

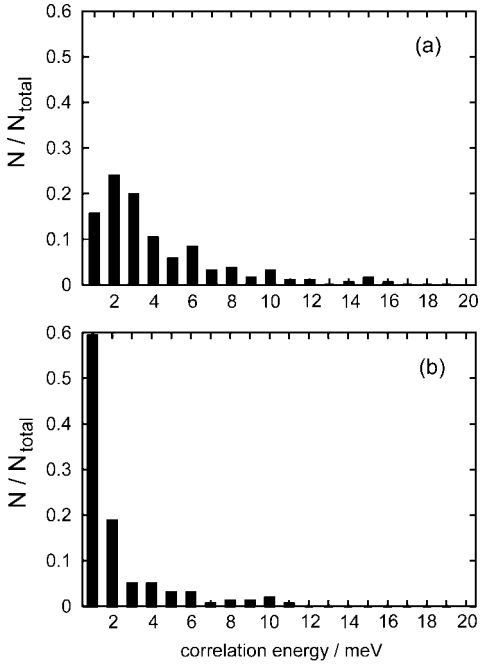

Figure 8. Histograms of MP2 SOMO pair correlation energies (SPCEs) for (a) $(H_2O)_{24}^-$ isomer $4^6 6^8$B and (b) $(H_2O)_{20}^-$ isomer 5^{14}. (Both histograms are normalized, so that what is plotted is the fraction of orbital pairs, N/N_{total}.) The surface state (b) shows a large number of orbitals with a very low SPCE, whereas the cavity state (a) shows a large number of orbitals with moderate SPCEs.

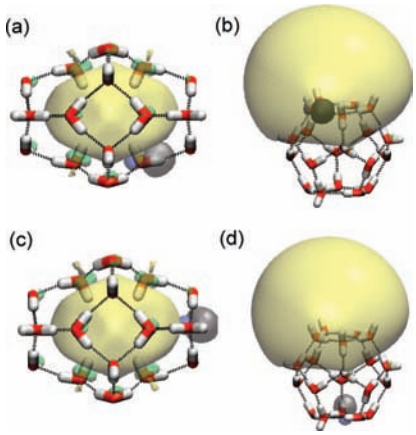

Figure 9. Boys-localized SOMOs (in yellow and green, representing positive and negative lobes) for a cavity state of $(H_2O)_{24}^-$ and a surface state of $(H_2O)_{20}^-$. In addition, (a) and (b) show the Boys orbitals that exhibit the largest SPCEs (in blue and gray), while (c) and (d) show the Boys orbitals exhibiting the smallest SPCEs (again in blue and gray).

between the SPCE and proximity of the orbital to the water molecules directly coordinated to the SOMO. Given this fact, it is perhaps surprising that the orbital with the highest SPCE is not localized mainly on the O−H bond of an H atom directly coordinated to the SOMO. The reason for this apparent anomaly would appear to be that the electron density along the O−H bond is itself folded into the SOMO. This is what gives the SOMO of the cavity state a bit of *p* character which, as seen in Figure 7a.

To verify that this interpretation is not simply a result of the high symmetry of the clathrate isomers, the same analysis was performed on a surface isomer and a cavity isomer taken from the QM/MM simulation. Two structures produced by carving out an $R = 4.5$ Å cluster from the QM/MM simulation (followed

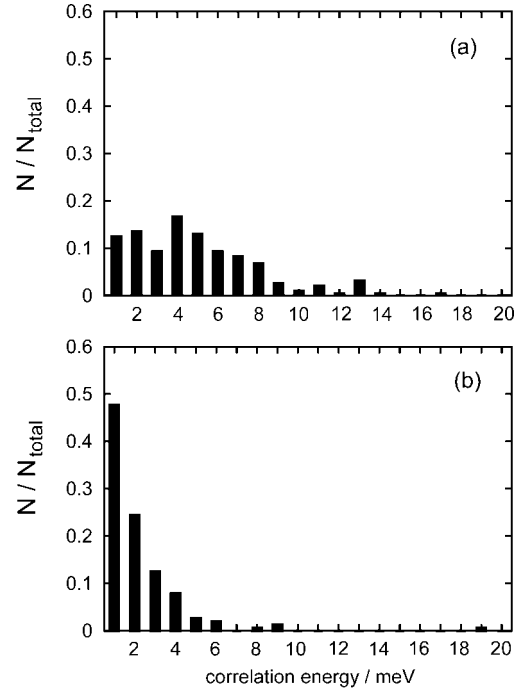

Figure 10. Histograms of MP2 SOMO pair correlation energies (SPCEs) for (a) an $n = 24$ cavity state and (b) an $n = 19$ surface state. (Both histograms are normalized, so that what is plotted is the fraction of orbital pairs, N/N_{total}.) Because the cavity isomer has a large number of water molecules packed into $R = 4.5$ Å there are many highly correlated orbitals.

by geometry optimization) are considered, one that forms a cavity state (Figure 7c) and another that forms a surface state (Figure 7d). The cavity state has a VEBE of 0.54 eV and the surface state has a VEBE of 0.21 eV. The total electron−water dispersion energy [defined in eq 7 as the sum of all SPCEs] is 0.84 eV for the cavity and 0.26 eV for the surface state. It is interesting to note that the surface state shows an AA binding motif wherein both the hydrogen atoms on one water molecule interact with the SOMO. Experiments have implicated such isomers in the vibrational spectroscopy of $(H_2O)_n^-$ clusters of this size, though to our knowledge no previous theoretical study has described AA isomers in clusters in this size regime.

A histogram of SPCEs for these isomers, calculated once again in the Boys-localized basis and depicted in Figure 10, shows the same trends that were observed for the high-symmetry clathrate structures, although the predominance of medium-sized SPCEs is even more pronounced for the cavity state in the present case. As can be seen in Figure 7c, the small radius of this isomer results in the dense packing of the water molecules about the SOMO, hence the large number of pairs with large SPCEs. For both the cavity-bound and the surface-bound isomers, the largest SPCE is several millielectronvolts larger than any of the other SPCEs.

The Boys-localized MOs with the highest and lowest SPCE for the two QM/MM cluster isomers are shown in Figure 11. For both the surface isomer and the cavity isomer, it is once again the case that the MO with the largest SPCE is localized on a water molecule that interacts directly with the SOMO, while the MO associated with the smallest SPCE is localized on a water molecule distant from the SOMO. In the case of the surface state (Figure 11b), the most highly-correlated MO is strongly localized on the water molecule displaying the AA motif. This has a much higher SPCE than the orbital with the second-largest SPCE (as can be seen in Figure 10), reflecting both its proximity to the SOMO and also its diffuseness.

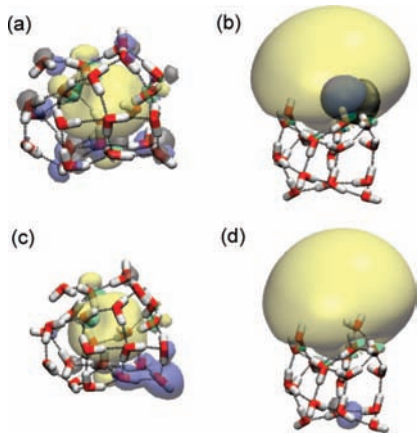

Figure 11. Boys-localized SOMOs (in yellow and green, representing positive and negative lobes) for a cavity state of $(H_2O)_{24}^-$ and a surface state of $(H_2O)_{19}^-$, extracted from a QM/MM simulation and then optimized. In addition, (a) and (b) show the Boys orbitals that exhibit the largest SPCEs (in blue and gray), and (c) and (d) show the Boys orbitals exhibiting the smallest SPCEs (again in blue and gray). The orbitals with a high SPCE are close to the SOMO whereas those with a low SPCE are distant from the SOMO. For the surface state, the orbital with the highest SPCE is strongly localized on the water with the AA motif.

IV. Conclusion

MP2 calculations for a large database of $(H_2O)_n^-$ isomers ($n = 14-33$) demonstrate that the correlation energy associated with the unpaired electron (equivalently, the portion of the VEBE arising from electron correlation) is greater for cavity isomers than it is for surface isomers. A decomposition of the MP2 correlation energy into pair correlation energies $E_{i,j}^{\mathrm{PCE}}$ (where i and j index occupied MOs) allows us to identify a certain part of the total correlation energy as electron−water dispersion. The electron−water dispersion energy is far larger for cavity-bound electrons than it is for surface-bound electrons. We have explained this effect using Boys localization[49] of the occupied MOs, for in this basis, the pair correlation energies $E_{i,\mathrm{SOMO}}^{\mathrm{PCE}}$ that contribute to electron−water dispersion decay with the distance between ϕ_i and the SOMO. As compared to surface states, cavity states simply have more occupied MOs in close proximity to the SOMO.

The observations above are a direct consequence of another important result: for surface states of $(H_2O)_n^-$, the SOMO shows very little penetration into the water cluster (hence the dearth of occupied MOs in close proximity to the SOMO). For example, in clathrate-type isomers of $(H_2O)_{20}^-$, isoprobability surfaces containing 99% of $|\phi_{\mathrm{SOMO}}|^2$ fail to penetrate into the interior of the cluster at all, resulting in fewer correlated pairs and thus a much smaller dispersion energy, relative to a cavity states of comparable size and VEBE. The reason for this lack of penetration is easily understood: stable, surface-bound electrons exist in large part due to stabilization of the excess electron by local dipole moments on individual water molecules whose dangling hydrogen atoms are oriented outward, away from the interior of the cluster. Such molecules provide no electrostatic driving force whatsoever that would promote penetration of the SOMO into the interior of the cluster. At the same time, the outward orientation of the hydrogen atoms puts most of the polarizable electron density of the water molecules at the surface (rather than the interior) of the cluster, so that electron−water dispersion also fails to provide a driving force for penetration, even though such dispersion certainly contributes to the VEBE, even for a surface state. In contrast, a cavity-bound electron has a strong driving force for outward penetration, which not only allows for favorable dispersion interactions with additional water molecules, but also decreases the curvature (and hence the kinetic energy) of the SOMO.

With regard to inspection of orbital isosurfaces for cavity-bound electrons, it is vital to know what fraction of the orbital density $|\phi(r)|^2$ is encapsulated by a given isosurface, and furthermore to choose a contour value that encompasses most (e.g., 90%) of $\int|\phi(r)|^2\,\mathrm{d}r$. In doing so, one discovers that the "solvated ball of charge" picture of the cavity states (suggested, e.g., by the SOMO plots in ref 20) is somewhat misleading, for in fact a nominally cavity-bound SOMO often penetrates far beyond the first solvation shell of water molecules. The usual approach to plotting orbital output from electronic structure programs—in which an isocontour value is selected arbitrarily, to produce a visually-appealing plot—can lead to a gross mischaracterization of the extent of the wavefunction.

Acknowledgment. This work was supported by an NSF CAREER award, by the ACS Petroleum Research Fund, and by start-up funds from The Ohio State University. Calculations ere performed at the Ohio Supercomputer Center. J.M.H. thanks Thomas Sommerfeld for finally goading him into calculating isoprobability surfaces.

Supporting Information Available: Geometries and energies for all $(H_2O)_n^-$ isomers considered here. This material is available free of charge via the Internet at http://pubs.acs.org.

References and Notes

(1) Coe, J.; Lee, G.; Eaton, J.; Arnold, S.; Sarkas, H.; Bowen, K. H.; Ludewigt, C.; Haberland, H.; Worsnop, D. R. *J. Chem. Phys* **1990**, *92* (6), 3980.
(2) Barnett, R. N.; Landman, U.; Cleveland, C. L.; Jortner, J. *J. Chem. Phys.* **1988**, *88*, 4429.
(3) Verlet, J. R. R.; Bragg, A. E.; Kammrath, A.; Cheshnovsky, O.; Neumark, D. M. *Science* **2005**, *307*, 93.
(4) Kim, J.; Park, J. M.; Oh, K. S.; Lee, J. Y.; Lee, S.; Kim, K. S. *J. Chem. Phys.* **1997**, *106*, 10207.
(5) Suh, S. B.; Lee, H. M.; Kim, J.; Lee, J. Y.; Kim, K. S. *J. Chem. Phys.* **2000**, *113*, 5273.
(6) Lee, H. M.; Suh, S. B.; Lee, J. Y.; Tarakeshwar, P.; Kim, K. S. *J. Chem. Phys.* **2000**, *112*, 9759.
(7) Lee, H. M.; Suh, S. B.; Kim, K. S. *J. Chem. Phys.* **2001**, *114*, 10749.
(8) Lee, H. M.; Lee, S.; Kim, K. S. *J. Chem. Phys.* **2003**, *119*, 187.
(9) Lee, H. M.; Suh, S. B.; Kim, K. S. *J. Chem. Phys.* **2003**, *118*, 9981.
(10) Wang, F.; Jordan, K. D. *J. Chem. Phys.* **2003**, *119*, 11645.
(11) Sommerfeld, T.; Gardner, S. D.; DeFusco, A.; Jordan, K. D. *J. Chem. Phys.* **2006**, *125*, 174301.
(12) Hammer, N. I.; Roscioli, J. R.; Johnson, M. A.; Myshakin, E. M.; Jordan, K. D. *J. Phys. Chem. A* **2005**, *109*, 11526.
(13) Hammer, N. I.; Shin, J. W.; Headrick, J. M.; Diken, E. G.; Roscioli, J. R.; Weddle, G. H.; Johnson, M. A. *Science* **2004**, *306*, 675.
(14) Hammer, N. I.; Roscioli, J. R.; Johnson, M. A. *J. Phys. Chem. A* **2005**, *109*, 7896.
(15) Hammer, N. I.; Roscioli, J. R.; Bopp, J. C.; Headrick, J. M.; Johnson, M. A. *J. Chem. Phys.* **2005**, *123*, 244311.
(16) Roscioli, J. R.; Hammer, N. I.; Johnson, M. A. *J. Chem. Phys. A* **2006**, *110*, 7517.
(17) Asmis, K. R.; Satambrogio, G.; Zhou, J.; Garand, E.; Headrick, J.; Goebbert, D.; Johnson, M. A.; Neumark, D. M. *J. Chem. Phys.* **2007**, *126*, 191105.
(18) Herbert, J. M.; Head-Gordon, M. *Proc. Natl. Acad. Sci. U.S.A.* **2006**, *103*, 14282.
(19) Khan, A. *J. Chem. Phys.* **2004**, *121*, 280.
(20) Herbert, J. M.; Head-Gordon, M. *J. Phys. Chem. A* **2005**, *109*, 5217.
(21) Herbert, J. M.; Head-Gordon, M. *Phys. Chem. Chem. Phys.* **2006**, *8*, 68.
(22) Coe, J. V.; Arnold, S. T.; Eaton, J. G.; Lee, G. H.; Bowen, K. H. *J. Chem. Phys.* **2006**, *125*, 014315.
(23) Khan, A. *J. Chem. Phys.* **2006**, *125*, 024307.
(24) Turi, L.; Madarasz, A.; Rossky, P. J. *J. Chem. Phys.* **2006**, *125*, 234707.
(25) Rossky, P.; Schnitker, J. *J. Chem. Phys.* **1988**, *92*, 4277.

(26) Wong, K. F.; Rossky, P. J. *J. Chem. Phys.* **2002**, *116*, 8418.
(27) Madarasz, A.; Rossky, P. J.; Turi, L. *J. Chem. Phys.* **2007**, *126*, 234707.
(28) Turi, L.; Sheu, W.; Rossky, P. *Science* **2005**, *309*, 914.
(29) Schnitker, J.; Rossky, P. *J. Chem. Phys.* **1987**, *86* (6), 3462.
(30) Barnett, R. N.; Landman, U.; Cleveland, C. L.; Jortner, J. *J. Chem. Phys.* **1988**, *88*, 4421.
(31) Turi, L.; Gaigeot, M. P.; Levy, N.; Borgis, D. *J. Chem. Phys.* **2001**, *114*, 7805.
(32) Turi, L.; Borgis, D. *J. Chem. Phys.* **2002**, *117*, 6186.
(33) Turi, L.; Sheu, W. S.; Rossky, P. J. *Science* **2005**, *310*, 914.
(34) Gutowski, M.; Skurski, P.; Boldyrev, A. I.; Simons, J.; Jordan, K. D. *Phys. Rev. A* **1996**, *54*, 1906.
(35) Gutowski, M.; Skurski, P. *J. Chem. Phys.* **1997**, *107*, 2968.
(36) Gutowski, M.; Skurski, P. *J. Phys. Chem. B* **1997**, *101*, 9143.
(37) Gutowski, M.; Jordan, K. D.; Skurski, P. *J. Phys. Chem. A* **1998**, *102*, 2624.
(38) Sommerfeld, T.; Jordan, K. D. *J. Am. Chem. Soc.* **2006**, *128*, 5828.
(39) Wang, F.; Jordan, K. D. *J. Chem. Phys.* **2002**, *116*, 6973.
(40) Gill, P. M. W.; Johnson, B. G.; Pople, J. A. *Chem. Phys. Lett.* **1993**, *209*, 506.
(41) Shao, Y.; Fusti-Molnar, L.; Jung, Y.; Kussmann, J.; Ochsenfeld, C.; Brown, S. T.; Gilbert, A. T. B.; Slipchenko, L. V.; Levchenko, S. V.; O'Neill, D. P.; Jr, R. A. D.; Lochan, R. C.; Wang, T.; Beran, G. J. O.; Besley, N. A.; Herbert, J. M.; Lin, C. Y.; Van Voorhis, T.; Chien, S. H.; Sodt, A.;; Steele, R. P.; Rassolov, V. A.; Maslen, P. E.; Korambath, P. P.; Adamson, R. D.; Austin, B.; Baker, J.; Byrd, E. F. C.; Dachsel, H.; Doerksen, R. J.;; Dreuw, A.; Dunietz, B. D.; Dutoi, A. D.; Furlani, T. R.; Gwaltney, S. R.;; Heyden, A.; Hirata, S.; Hsu, C.-P.; Kedziora, G.; Khalliulin, R. Z.; Klunzinger, P.; Lee, A. M.; Lee, M. S.; Liang, W.; Lotan, I.; Nair, N.; Peters, B.; Proynov, E. I.; Pieniazek, P. A.; Rhee, Y. M.; Ritchie, J.; Rosta, E.; Sherrill, C. D.; Simmonett, A. C.; Subotnik, J. E.; Woodcock, H. L.; Zhang, W.; Bell, A. T.; Chakraborty, A. K.; Chipman, D. M.; Keil, F. J.; Warshel, A.; Hehre, W. J.; Schaefer, H. F.; Kong, J.; Krylov, A. I.; Gill, P. M. W.; Head-Gordon, M. *Phys. Chem. Chem. Phys.* **2006**, *8*, 3172.
(42) Schaftenaar, G.; Noordik, J. *J. Comput.-Aided Mol. Design* **2000**, *14*, 123.
(43) Humphrey, W.; Dalke, A.; Schulten, K. *J. Mol. Graph.* **1996**, *14*, 33.
(44) There is a sign error in the definition of Δ in our previous work (ref 21), but the signs of the data given in that reference reflect the sign convention used here, in which $\Delta > 0$.
(45) Jeffrey, G. A. In *Inclusion Compounds*; Atwood, J. L., Davies, J. E. D., MacNichol, D. D., Eds.; Academic Press: New York, 1984; *Vol. 1*, p 135.
(46) Bartels, D. M. *J. Chem. Phys.* **2001**, *115*, 4404.
(47) Ayotte, P.; Johnson, M. A. *J. Chem. Phys.* **1997**, *106*, 811.
(48) Kosloff, D.; Kosloff, R. *J. Comput. Phys.* **1983**, *52*, 35.
(49) Boys, S. F. *Rev. Mod. Phys.* **1960**, *32*, 296.

JP802272R